Published in final edited form as:

Nat Med. 2018 May ; 24(4): 401–407. doi:10.1038/nm.4513.

A public antibody lineage that potently inhibits malaria infection by dual binding to the circumsporozoite protein

Joshua Tan[1,2,*], **Brandon K Sack**[3,*], **David Oyen**[4,*], **Isabelle Zenklusen**[5,6,*], **Luca Piccoli**[1,*], **Sonia Barbieri**[1], **Mathilde Foglierini**[1,7], **Chiara Silacci Fregni**[1], **Jessica Marcandalli**[1], **Said Jongo**[8], **Salim Abdulla**[8], **Laurent Perez**[1], **Giampietro Corradin**[9], **Luca Varani**[1], **Federica Sallusto**[1,10], **B Kim Lee Sim**[11], **Stephen L Hoffman**[11], **Stefan H I Kappe**[3], **Claudia Daubenberger**[5,6,§], **Ian A Wilson**[4,12,§], and **Antonio Lanzavecchia**[1,10,§]

[1]Institute for Research in Biomedicine, Università della Svizzera Italiana, Via Vincenzo Vela 6, 6500 Bellinzona, Switzerland [2]Radcliffe Department of Medicine, University of Oxford, John Radcliffe Hospital, Headington, Oxford, OX3 9DS, UK [3]Center for Infectious Disease Research, 307 Westlake Avenue North, Seattle, WA 98109, USA [4]Department of Integrative Structural and Computational Biology, The Scripps Research Institute, La Jolla, CA 92037, USA [5]University of Basel, Petersplatz 1, 4003 Basel, Switzerland [6]Swiss Tropical and Public Health Institute, Clinical Immunology Unit, 4002 Basel, Switzerland [7]Swiss Institute of Bioinformatics (SIB), Lausanne, Switzerland [8]Ifakara Health Institute, Bagamoyo Clinical Trial Unit, P.O. Box 74, Bagamoyo, Tanzania [9]Biochemistry Department, University of Lausanne, Chemin des Boveresses 157, 1066 Epalinges, Switzerland [10]Institute for Microbiology, ETH Zurich, Wolfgang-Pauli-Strasse 10, 8093 Zurich, Switzerland [11]Sanaria Inc., Rockville, Maryland 20850, USA [12]The Skaggs Institute for Chemical Biology, The Scripps Research Institute, La Jolla, CA, USA

Abstract

Immunization with attenuated *Plasmodium falciparum* sporozoites (PfSPZ) has been shown to be protective, but the features of the antibody response induced by this treatment remain unclear. To

Correspondence: lanzavecchia@irb.usi.ch.

*These authors contributed equally to this work

§These authors jointly supervised this work

Supplementary information is available on the online version of the paper.

Author Contributions J.T. characterized monoclonal antibodies, analyzed the data and wrote the manuscript; B.K.S. performed *in vivo* assays, analyzed the data and wrote the manuscript; D.O. performed structural analysis, analyzed the data and wrote the manuscript; I.Z. collected samples, conducted *in vitro* assays, analyzed the data and wrote the manuscript; L.Pi. characterized monoclonal antibodies, analyzed the data and wrote the manuscript; S.B. sequenced and expressed antibodies; M.F. performed bioinformatics analysis; C.S.F. immortalized memory B cells; J.M and L.Pe. immunized mice; S.J. supervised cohorts; S.A. oversaw the clinical trial and provided PBMCs to the laboratory team; G.C. provided PfCSP peptides; L.V. designed peptide and antibody mutants; F.S. and S.H.I.K. provided supervision; S.L.H. and B.K.L.S. produced PfSPZ Vaccine and PfCSP, prepared the syringes used to immunize, and provided PfSPZ for antibody assays, including screening of mAbs; C.D. handled cohorts and provided supervision; I.A.W. supervised structural analysis and wrote the manuscript; A.L. provided overall supervision, analyzed the data and wrote the manuscript.

Competing Financial Interests A.L. is the scientific founder and shareholder of Humabs BioMed. F.S. is a shareholder of Humabs BioMed. Sanaria Inc. manufactured PfSPZ Vaccine and PfSPZ Challenge.

investigate this response at high resolution, we isolated IgM and IgG monoclonal antibodies from Tanzanian volunteers who were immunized by repeated injection of irradiated PfSPZ and who were found to be protected from controlled human malaria infection (CHMI) with infectious homologous PfSPZ. All IgG monoclonals isolated bound to *P. falciparum* circumsporozoite protein (PfCSP) and recognized distinct epitopes in the N-terminus, NANP repeat region, and C-terminus. Strikingly, the most effective antibodies, as assessed in a humanized mouse model, bound not only to the repeat region, but also to a minimal peptide at the PfCSP N-terminal junction that is not in the RTS,S vaccine. These dual-specific antibodies were isolated from different donors and used VH3-30 or VH3-33 alleles carrying tryptophan or arginine at position 52. Using structural and mutational data, we describe the elements required for germline recognition and affinity maturation. Our study provides potent neutralizing antibodies and relevant information for lineage-targeted vaccine design and immunization strategies.

Malaria is a serious global health threat, causing 445,000 deaths and 216 million clinical cases in 2016[1]. Much of the effort to develop a vaccine against the disease has focused on *Plasmodium falciparum* sporozoites (PfSPZ), the asymptomatic parasite stage that is injected by mosquitoes into the host skin to initiate a malaria infection. After entering the skin, PfSPZ migrate to the liver, multiply in hepatocytes and then emerge in the blood, where the parasites cause malaria symptoms and differentiate into sexual stages for transmission. While natural infection by PfSPZ elicits little or no protective immunity to this stage of the life cycle[2,3], subunit or whole organism vaccines based on PfSPZ can induce robust immune responses[4–6]. The most advanced malaria vaccine candidate, RTS,S, incorporates part of the *P. falciparum* circumsporozoite protein (PfCSP), which coats the PfSPZ surface and plays a key role in parasite migration out of the skin, entry into the liver parenchyma and invasion of hepatocytes[7–12]. Multi-site clinical trials in sub-Saharan Africa have shown that RTS,S confers significant but modest and short-lived protection against clinical illness[10,13,14]. An alternative approach that has shown promise is the use of whole attenuated PfSPZ as immunogens. This line of research is based on key early discoveries that immunization with irradiated *P. berghei* sporozoites protected mice against subsequent challenge[15] and that immunization of humans with >1000 irradiated mosquitoes carrying PfSPZ conferred sterilizing protection against controlled human malaria infection (CHMI)[16–18]. These studies have led to efforts to develop whole attenuated PfSPZ as a vaccine[19], and recent trials have shown that immunization with attenuated PfSPZ was highly protective in malaria-naïve volunteers and gave significant protection in Malian adults[6,20–22]. While these results are promising, the specific mediators of this protective immune response have yet to be fully elucidated. Studies of the antibody response have mainly investigated polyclonal serum responses to PfSPZ and PfCSP[6,20–22], and high-resolution analysis of the monoclonal antibodies generated by vaccination and their target antigens on the PfSPZ surface remains to be performed. These experiments could provide useful information for the improvement of whole sporozoite-based vaccines and for the identification of new antigens as subunit vaccine candidates, as well as to generate tools for prophylaxis of *P. falciparum* infection.

Malaria-exposed individuals produce robust antibody responses to immunizations with PfSPZ Vaccine

We characterized the antibody response of Tanzanian volunteers living in malaria-endemic regions who were immunized by repeated intravenous injection of irradiated PfSPZ (PfSPZ Vaccine) and then underwent CHMI with live homologous parasites (Fig. 1a). Serum IgM and IgG antibodies, as measured by flow cytometry on live PfSPZ, increased following immunization, but did not show a clear association with protection from CHMI (Fig. 1b,c and Supplementary Fig. 1a,b). Memory B cells from five protected individuals were immortalized and screened by staining of intact PfSPZ to isolate human monoclonal antibodies against any surface antigen on PfSPZ (Supplementary Fig. 1c). Most of the IgG monoclonal antibodies bound to PfSPZ with high affinity (Fig. 1d,e). Interestingly, in the two donors from whom both PfSPZ-specific IgM and IgG monoclonal antibodies were isolated, the IgM antibodies were recovered at much higher numbers (Fig. 1f). The IgM antibodies had fewer, but still substantial, mutations compared to the IgG antibodies, consistent with an origin from IgM memory B cells (Fig. 1g). In particular, the finding of an antibody lineage containing both IgM and IgG members suggests an incomplete switch in this response despite repeated immunization (Supplementary Fig. 1d). These results demonstrate that immunizations with PfSPZ Vaccine induce a robust antibody response that retains a significant IgM component.

PfSPZ-specific monoclonal antibodies exhibit potent neutralizing capacity *in vitro* and *in vivo*

To identify the features of the most effective neutralizing monoclonal antibodies produced by the protected individuals, we tested a panel of IgG antibodies *in vitro* for their capacity to inhibit PfSPZ traversal and invasion of a human hepatocyte cell line (Fig. 2a). The invasion-inhibitory activity varied among antibodies and was significantly correlated with binding affinity to PfSPZ (Fig. 2b). A subset of antibodies was further tested in an *in vivo* mouse humanized liver model for their capacity to protect against natural, mosquito bite-transmitted infection by PfSPZ. Some antibodies, such as MGG3, MGG4, MGH2, MGU10 and MGU12, were very potent in reducing liver burden by up to 98.3%, while others, such as MGG8, MGH1, MGH3 and MGU1, were less effective (Fig. 2c). These findings suggest that *in vivo* neutralizing activity may be related to the fine specificity of the antibodies.

Highly neutralizing antibodies exhibit dual specificity for NANP and the N-terminus junction of PfCSP and show common usage of VH3-30^{f} genes

Next, we set out to identify the target antigens of the monoclonal antibodies. Strikingly, although we had used an antigen-agnostic approach to identify antibodies that bound to the PfSPZ surface regardless of specificity, we found that all of the antibodies bound to recombinant PfCSP (Fig. 2d,e), confirming that this is the most immunogenic protein on the PfSPZ surface[23–25]. To understand the basis for effective neutralization, we mapped the specificity of the monoclonal antibodies using synthetic peptides that cover the N-terminus, the NANP repeat region, the N-terminal junction (connecting region between the N-terminal

domain and NANP repeats), and the C-terminus of PfCSP. Binding to the classical NANP repeats (NANP18 peptide), the PfCSP C-terminus, recombinant PfCSP or PfSPZ did not correlate with efficacy (Supplementary Fig. 2a–d). Interestingly, however, binding to a minimal 15-mer peptide (NPDP15) that covers the junction between the N-terminal domain and the NANP repeats was a shared characteristic of the most potent *in vivo* neutralizing antibodies (Fig. 2f). These potent antibodies also recognized the NANP18 peptide, suggesting that the capacity to bind both to the NANP repeats and to the N-terminal junction of PfCSP is the main feature of efficient neutralization. Another distinctive characteristic of the most potent antibodies was the common usage of VH3-30 family alleles carrying tryptophan or arginine at position 52 (VH3-30^{f}, here defined as including VH3-30, VH3-30-3, VH3-30-5 and VH3-33 alleles sharing >96% identity) (Fig. 2e, Supplementary Fig. 3,4, Supplementary Table 1). Strikingly, VH3-30^{f} was the most common VH gene used by IgM antibodies isolated from donors G and U, with almost 90% of such antibodies carrying W52 or R52 (Supplementary Fig. 2e). Collectively, these data indicate that the most potent antibodies have a dual specificity and share common VH gene usage. Importantly, such antibodies were isolated from four out of five donors, suggesting that these antibodies belong to a public lineage and therefore have the potential to be readily induced by vaccination.

VH3-30^{f} antibodies acquire dual specificity and high affinity for PfCSP through somatic mutations

To investigate the influence of somatic mutations on binding of VH3-30^{f} antibodies to PfCSP, we focused on two clonally related and highly mutated antibodies, MGU1 and MGU10 (Fig. 3a). The unmutated common ancestor (UCA) of these antibodies, which carries tryptophan at position 52, was able to bind to PfCSP and PfSPZ with low affinity, while substitution to serine 52, which is commonly found in VH3-30 alleles, resulted in loss of binding (Fig. 3b,c). These findings, in conjunction with the high frequency of W52 in the IgM sequences and the identification of putative VH3-30^{f} alleles carrying W52 in the germline sequences obtained from non-B cells of donors G, U and W (Supplementary Fig. 3,4), identify VH3-30^{f} alleles carrying W52 as a preferred feature for the initiation of this lineage-specific antibody response to PfCSP. The branch point of this clone achieved, through several mutations, high affinity binding to PfSPZ, PfCSP and NANP18, while further mutations in MGU10, but not MGU1, increased breadth by conferring the unique ability to bind to NPDP15 (Fig. 3b–e, Supplementary Fig. 5). Despite their similarities in binding to PfSPZ, PfCSP and NANP18, MGU10 was substantially more potent than MGU1 in the *in vivo* assay (Fig. 2c), suggesting that acquisition of binding to NPDP15 is the key factor for potent neutralization. Interestingly, mutagenesis studies of MGU10 suggest that W52 remains a critical residue for binding to NPDP15, but becomes dispensable for high affinity binding to NANP and full-length PfCSP in the fully mutated antibody (Fig. 3f). In contrast, in a second clonal family consisting of MGU5 and MGU8, full binding to PfCSP, NANP18, NPDP15 and PfSPZ was already achieved by the branch point while the remaining mutations appeared redundant (Supplementary Fig. 6a–e).

Unmutated VH3-30^{f} antibodies recognize PfCSP NANP repeat units and subsequently acquire binding to specific motifs in the N-terminal junction

To investigate the original specificities of germline VH3-30^{f} antibodies, we analysed binding of the UCAs of various VH3-30^{f} antibodies to PfCSP peptides using a more sensitive bead-based assay. Most UCAs bound to NANP18 but not to NPDP15, suggesting that the antibodies generally started as NANP-specific and gained affinity for NPDP15 through somatic mutations (Supplementary Fig. 6f–m). These data delineate a pathway of antibody development that is dependent on specific VH alleles and leads to antibodies with dual specificity. To identify the minimal residues recognized by antibodies at the PfCSP N-terminal junction, we performed a mutational analysis on NPDP19, a 19-mer version of NPDP15 that was used to provide a longer scaffold for binding (Fig. 3g). The loss of binding to certain peptides identified a specific motif (DPNANP) that was recognized by most antibodies regardless of VH gene usage. These findings, combined with data from peptide array experiments (Supplementary Fig. 7), identify the N-terminal junction binding site of the most potent neutralizing antibodies as including the first unit of the NANP repeat region and flanking non-repeat sequences, providing a molecular basis for the dual specificity of these antibodies.

Structural analysis of the MGG4 antibody reveals the basis for recognition of the PfCSP N-terminal junctional peptide

To gain structural insights into the recognition of the N-terminal junction, we attempted to crystallize several VH3-30^{f} antibodies and successfully crystallized MGG4 in complex with the Ac-^{1}KQPADGNPDPNANP^{14}-NH_2 peptide (Fig. 4a **and** Supplementary Table 2). Only the C-terminal half (NPDPNAN, residues 7–13) of the peptide was visible, with most of the contacts being made by heavy-chain residues as shown by the Fab buried surface area (Fig. 4b). Specifically, the heavy-chain CDR loops form a groove in which the peptide resides (Fig. 4a **and** Supplementary Fig. 8a). In addition, three interfacial waters are involved in an extensive hydrogen-bonding network, connecting the side chain of N11 to the base of CDR H1 and CDR H3 (Supplementary Fig. 8b). The CH/**π** interaction between P10 and W52 (Fig. 4a **and** Supplementary Fig. 8b) confirms that the latter residue is critical for binding as indicated by the mutagenesis experiments. While most peptide residues, except for N13, display a relatively large buried surface area (Fig. 4c), weak electron density for the residues visible at the peptide's termini (N7, P8, A12 and N13) (Fig. 4e **and** Supplementary Fig. 8c) indicates structural flexibility and highlights the sequence DPN as the principal binding motif. Interestingly, the DPN sequence displays a pseudo 3_{10} turn, which is stabilized by hydrogen bonding of the aspartate side chain to the asparagine backbone amide. Such a conformation is very similar to turns observed for unbound NANP peptides in solution and in crystal structures of free and antibody-bound peptides (Fig. 4d)[25–29]. An isolated DPN motif is also present in the 282–383 C-terminal peptide, which may explain its binding to MGG4 (Fig. 2e), notwithstanding the significant differences between the DPN flanking residues in the 282–383 C-terminal and the N-terminal junctional peptides (**N**DPN**R** versus **P**DPN**A**, respectively). Binding to both NPDP and NANP repeats suggests that the aspartate residue in the DPN motif is interchangeable with an asparagine. Binding studies of MGG4

to NPDP19 peptide mutants validate the specificity of MGG4 toward DPN and NPN motifs (Fig. 3g). Only when the central DPN and NPN motifs within the NPDP19 peptide are mutated to DPA and AAN is MGG4 binding completely abrogated. In contrast, a third DPN motif present at the C-terminus of the NPDP19 peptide does not contribute to binding, possibly indicating the importance of flanking residues for optimal binding. Overall, these data imply that potential peptide-binding promiscuity allows MGG4 to bind to diverse epitopes on PfCSP. Since other VH3-30^{f} antibodies cannot bind to the 282–383 peptide, we expect that they will be less promiscuous and bind slightly larger or more specific sequences.

Immunization of mice with the NPDP19 peptide generates a robust but non-inhibitory anti-PfSPZ response

The finding that the most potent monoclonal antibodies recognize a defined N-terminal junctional peptide suggests that this region could be a component of an effective subunit vaccine. In an initial attempt to investigate whether the NPDP19 peptide might be sufficient to induce a protective response, we immunized BALB/c mice with NPDP19 conjugated to KLH. All mice produced IgG antibodies that were specific for the NPDP19 peptide, but were at best weakly reactive for the NANP18 peptide (Supplementary Fig. 9a,b). Strikingly, in spite of their ability to bind to PfSPZ, the mouse sera were unable to inhibit PfSPZ invasion of a hepatocyte cell line *in vitro*, suggesting that dual specificity for NANP and the N-terminal junction may be required for potent neutralizing function (Supplementary Fig. 9c,d). The reliance of the dual-specific antibodies that we isolated on specific human VH3-30^{f} alleles suggests that mice, which do not have the counterparts of human VH3-30^{f} genes, may not be the most suitable model organism to test a novel CSP-based vaccine. Rather, an organism such as the *Aotus* monkey, which has a more similar VH gene repertoire to humans and contains VH3-30^{f}-like genes carrying the equivalent of W52[30], may be a more suitable choice.

Discussion

This study shows that the antibodies produced by vaccinated and protected African individuals contain a highly mutated IgG component, as well as an important IgM component with fewer but substantial mutations, as also seen in the response to blood-stage *Plasmodium* antigens[31]. The large IgM component would be consistent with stimulation of marginal zone B cells in the spleen following intravenous immunization with a particulate antigen[32]. Strikingly, all of the IgG antibodies that we identified recognized PfCSP, consistent with previous studies describing the immunodominance of this protein and its abundance on the PfSPZ surface[23–25,33,34]. Our findings are in agreement with previous work that separately describes the importance of the PfCSP NANP repeat region and of the N-terminus[23,35–37], but, importantly, highlight the fact that antibodies that target epitopes in both regions simultaneously are more potent than antibodies that exclusively recognize each individual site. Interestingly, the structural analysis and peptide mutational data indicate that these antibodies, which are originally specific for NANP motifs, do not acquire a completely unrelated specificity, but rather gain promiscuity for sequences centred on a DPN motif. This

dual specificity is to a large extent encoded by VH3-30[f] alleles, but also requires extensive somatic mutations. The importance of dual specificity is highlighted by the fact that immunization with a single NPDP19 peptide is not sufficient to confer protection despite eliciting PfSPZ-binding antibodies.

The increased potency of the dual-specific antibodies could be due to the proximity of the N-terminal junction to region I (KLKQP) of PfCSP, which is involved in the cleavage of the N-terminus to allow PfSPZ invasion of hepatocytes[9,12]. This N-terminal junction region is not included in the most advanced malaria vaccine candidate RTS,S, which may explain its limited efficacy in malaria-endemic regions[10]. These findings support continued work to develop whole PfSPZ vaccines, which contain the entire PfCSP, and provide a rationale for further attempts to develop refined vaccination approaches to elicit dual-specific antibodies using prime-boost strategies with improved carriers[38,39].

The finding that the most potent antibodies share common VH gene usage in multiple donors is consistent with a public antibody response that can be readily induced by vaccination. These results are reminiscent of previous work on the use of particular VH genes and their allelic forms in the response to the stem of influenza haemagglutinin[40,41] and justify further efforts to investigate the role of VH gene polymorphisms in protective antibody responses. Nevertheless, whether these antibodies are sufficient to protect humans and why some individuals were not protected remain to be established. Possible reasons for the latter include the lack of a VH3-30[f] allele, the incomplete maturation of the VH3-30[f] antibodies, or insufficient production of the potent antibodies. The antibodies described could be used to obtain proof of concept that antibodies alone can be protective *in vivo* in humans, as previously shown in mice and non-human primates[42–44], and pave the way for the use of antibodies in the prophylaxis of *P. falciparum* infection and for the development of improved antibody-based subunit malaria vaccines.

Methods

Sporozoites

Aseptic, purified cryopreserved PfSPZ of the NF54 strain provided by Sanaria® were used in serum and monoclonal antibody binding experiments. PfSPZ produced by the Center for Infectious Disease Research, Seattle was used in all *in vitro* and *in vivo* functional assays.

Clinical trial and donors

Following informed consent, blood samples used in this study were collected from malaria pre-exposed volunteers during a clinical phase 1 clinical trial of the safety, immunogenicity and protective efficacy of the Sanaria® PfSPZ Vaccine in Bagamoyo, Tanzania between 2014 and 2015. The trial was performed in accordance with Good Clinical Practices and the protocol was approved by Institutional Review Board of the Ifakara Health Institute (IHI-IRB) (Ref. No. IHI/IRB/No:02-2014), the National Institute for Medical Research Tanzania (NIMR/HR/R.8a/Vol.IX/1691) and the Ethikkommission Basel (EKNZ), Basel, Switzerland (reference number 261/13). The protocol was approved by the Tanzania Food and Drug Authority (TFDA) (Ref. No. TFDA13/CTR/0003), registered at Clinical Trials.gov

(NCT02132299) and conducted under U.S. FDA IND 14826. Detailed information on the study procedures of the trial are given in Jongo *et al.* 2017 (manuscript submitted). Briefly, healthy male volunteers aged 20–30 years were randomized to direct venous inoculation (DVI) of 5 doses of normal saline or 1.35×10^5 or 2.7×10^5 PfSPZ of the Sanaria® PfSPZ Vaccine. Vaccine efficacy was assessed by homologous controlled human malaria infection (CHMI) by DVI inoculation of 3,200 infectious PfSPZ Challenge, at 3 and 24 weeks after the last PfSPZ vaccination.

Sample collection and preparation

For serum preparation, whole blood was collected in Vacutainer tubes (BD) containing clot activators and kept at room temperature until a clot was formed. The tube was centrifuged at 2,000 × *g* for 10 min at 22°C and the serum fraction was stored at −80°C. Peripheral blood mononuclear cells (PBMCs) were isolated from whole blood by Ficoll density gradient centrifugation and resuspended in freezing medium for long-term storage in liquid nitrogen.

Flow cytometry assay to detect antibody binding to PfSPZ

Cryopreserved PfSPZ (Sanaria®) were thawed and stained with different concentrations of Tanzanian sera or monoclonal antibodies in 3.3× SYBR Green I (ThermoFisher Scientific) for 30 min at 4°C. The PfSPZ were washed twice by centrifugation at 3220 × g for 5 min. Human serum antibody binding was detected using 2.5 μg ml^{-1} Alexa Fluor 647-conjugated goat anti-human IgG (Jackson ImmunoResearch, 109-606-170) or Alexa Fluor 647-conjugated goat anti-human IgM (Jackson ImmunoResearch, 109-606-129). Mouse serum antibody binding was detected using 1 μg ml^{-1} PE-Cy7-conjugated goat anti-mouse IgG (Biolegend, 405315) or PE-Cy7-conjugated rat anti-mouse IgM (BD Biosciences, 552867). FACS Diva (version 6.2) was used for acquisition of samples and Flow-Jo (version 10.1) was used for FACS analysis. The PfSPZ were gated based on high fluorescence in the FITC channel. Median fluorescence intensity (MFI) of the PfSPZ in the Alexa Fluor 647 or PE-Cy7 channel was calculated to quantify IgG or IgM binding. The concentration of antibody needed to achieve MFI 10,000 ($Conc_{10000}$) was calculated by interpolation of binding curves fitted to a sigmoidal curve model (Graphpad Prism 7) as a measure of affinity. The gating strategy can be found in Supplementary Figure 1.

B-cell immortalization and isolation of monoclonal antibodies

IgM or IgG memory B cells were isolated from frozen peripheral blood mononuclear cells (PBMCs) by magnetic cell sorting with 0.5 μg ml^{-1} anti-CD19-PECy7 antibodies (BD, 341113) and mouse anti-PE microbeads (Miltenyi Biotec, 130-048-081), followed by FACS sorting using 3.75 μg ml^{-1} Alexa Fluor 647-conjugated goat anti-human IgG (Jackson ImmunoResearch, 109-606-170), 5 μg ml^{-1} Alexa Fluor 647-conjugated goat anti-human IgM (Invitrogen, A21215) and 1/40 PE-labeled anti-human IgD (BD, 555779). As previously described[47], sorted B cells were immortalized with Epstein-Barr virus (EBV) and plated in single cell cultures in the presence of CpG-DNA (2.5 μg ml^{-1}) and irradiated PBMC-feeder cells. Two weeks post-immortalization, the culture supernatants were tested (at a 2/5 dilution) for binding to PfSPZ by flow cytometry using a no-wash protocol. Briefly, cryopreserved PfSPZ were thawed, stained with the supernatants in 6.25× SYBR Green I for 30 min at room temperature, and incubated with 2.5 μg ml^{-1} Alexa Fluor 647-conjugated

goat anti-human IgG or anti-human IgM for 1 hour at 4°C. Only supernatants that did not bind to control beads were selected to exclude polyreactive antibodies.

In vitro inhibition of PfSPZ invasion and traversal

The ability of monoclonal antibodies and serum to prevent PfSPZ invasion and traversal *in vitro* was tested as previously described[44,48]. Briefly, monoclonal antibodies at 10 μg ml^{-1} were mixed with freshly dissected PfGFP_luc sporozoites in DMEM media containing FITC-dextran, 10% FBS, pen/strep, fungizone and L-glutamine and incubated at 37°C for 15 min. These PfSPZ were then added to HC04 hepatoma cells plated one day prior at 80,000 cells/well in a 96-well plate for a final MOI of 0.3 (26,000 PfSPZ: 80,000 HC04). Plates were then spun at 500 × g for 3 min and the PfSPZ were left to infect for 90 min at 37°C. Cells were then fixed, stained with 10 μg ml^{-1} of the monoclonal antibody 2A10 conjugated to AlexaFluor-647 and analyzed by flow cytometry for invaded cells (2A10/AlexaFluor-647 positive) or traversed cells (FITC-dextran positive).

In vivo P. falciparum mosquito bite challenge in humanized liver mice

FRG huHep mice were purchased from Yecuris, Inc. and infected by bite of 50 PfGFP_luc mosquitos 16–24 hours following intraperitoneal injection of 150 μg/mouse of each monoclonal antibody or human IgG control as described previously[44]. Parasite liver burden was determined by bioluminescent imaging using an IVIS imager at day 6 at the peak of liver burden. Reductions in liver burden were calculated by normalization to the mean of control mice injected with an equivalent dose of human IgG within each bite experiment. All animal procedures were conducted in accordance with and approved by the Center for Infectious Disease Research Institutional Animal Care and Use Committee (IACUC) under protocol SK-16. The Seattle Biomed IACUC adheres to the NIH Office of Laboratory Animal Welfare standards (OLAW welfare assurance # A3640-01).

Sequence analysis of antibody cDNA

cDNA was synthesized from selected B-cell cultures and both heavy chain and light chain variable regions (VH and VL) were sequenced as previously described[49]. The usage of VH and VL genes and the number of somatic mutations were determined by analyzing the homology of VH and VL sequences of monoclonal antibodies to known human V, D and J genes in the IMGT database (version 3.4.8)[50]. Antibody-encoding sequences were amplified and sequenced with primers specific for the V and J regions of the given antibody. Sequences were aligned with Clustal Omega (version 1.2.4)[51]. Unmutated common ancestor (UCA) sequences of the VH and VL were inferred with Antigen Receptor Probabilistic Parser (ARPP) UA Inference software, as previously described[52], or constructed using IMGT/V-QUEST[50]. Phylogenetic trees were generated with the DNA Maximum Likelihood program (Dnaml) of the PHYLIP package, version 3.69[40,53].

Production of recombinant antibodies and antibody variants

Antibody heavy and light chains were cloned into human IgG1, Igκ and Igλ expression vectors and expressed by transient transfection of Expi293F Cells (ThermoFisher Scientific)

using polyethylenimine. Cell lines were routinely tested for mycoplasma contamination. The antibodies were affinity purified by protein A chromatography (GE Healthcare).

X-ray crystallography

The KQPADGNPDPNANP peptide was ordered from Innopep Inc. with a purity of >98% and containing chlorine counter ions. The peptides have N-terminal acetylation and C-terminal amidation to eliminate charges at the peptide termini. The MGG4-peptide complex was crystallized from a solution containing MGG4 at 11.4 mg ml^{-1} in TBS buffer (50 mM Tris-HCl, 137 mM NaCl, 2.7 mM KCl, pH 8.0) with a 5:1 molar ratio of Ac-KQPADGNPDPNANP-NH_2 peptide to Fab. Crystals were grown using sitting drop vapor diffusion with a well solution containing 0.04 M KH2PO4, 20% glycerol, 16% PEG8000 at 277 K and typically appeared within 3 days. Crystals were cryo-cooled without additional cryoprotection. X-ray diffraction data were collected at the Advanced Light Source (ALS) 5.0.3. Data collection and processing statistics are outlined in Supplementary Table 2. Data sets were indexed, integrated, and scaled using the HKL-2000 package (version 712)[54]. The structures were solved by molecular replacement using PHASER (version 2.7.17)[55] with a homology model (SWISS-MODEL[56–58] and PIGSPro[59]) for MGG4 as a search model. After refinement of the Fab using phenix.refine (version 1.12-2829)[60] combined with additional manual building cycles in Coot (version 0.8.8)[61], positive Fo-Fc density was observed in the Fab combining site for the peptide. The peptide was manually built into the difference density Fo-Fc map, followed by additional rounds of refinement of the complex in phenix.refine[60] and manual building cycles in Coot[61]. Buried surface areas (BSA) were calculated with the program MS (version 1.0)[62], using a 1.7-Å probe radius and standard van der Waals radii[63].

ELISA

Total IgGs were quantified using half-area, high-binding 96-well plates (Corning) with 10 μg ml^{-1} goat anti-human IgG (SouthernBiotech, 2040-01) using Certified Reference Material 470 (ERMs-DA470, Sigma-Aldrich) as a standard. To test specific antibody binding, ELISA plates were either directly coated with 1 μg ml^{-1} of recombinant PfCSP (Sanaria®, sequence previously shown[21]), 2 μg ml^{-1} of peptide 22–110 or 1 μg ml^{-1} of peptide 282–383, or first with 10 μg ml^{-1} of avidin (Sigma-Aldrich), followed by 10 μg ml^{-1} of NANP18 (NANPNANPNANPNANPNA), NPDP19 (KQPADGNPDPNANPNVDPN), NPDP15 (KQPADGNPDPNANPN) or various NPDP19 peptide mutants. Non-specific binding to plates coated with an irrelevant control peptide was tested to exclude polyreactivity of the antibodies. All peptides and mutants were synthesized with biotin attached to the C-terminus (A&A Labs). Plates were blocked with 1% bovine serum albumin (BSA) and incubated with titrated antibodies, followed by 1/500 AP-conjugated goat anti-human IgG (Southern Biotech, 2040-04). Plates were then washed, substrate (p-NPP, Sigma) was added and plates were read at 405 nm.

Bead-based assay to detect binding to PfCSP peptides

Streptavidin beads with different levels of FITC labelling (SVFB-2552-6K, Spherotech) were coated with 10 μg ml^{-1} of biotinylated NANP18, NPDP15, NPDP19 or a negative control peptide for 30 min at room temperature. The beads were washed and incubated with

titrations of monoclonal antibodies for 20 min at room temperature. Antibody binding was detected with 2.5 μg ml^{-1} Alexa Fluor 647-conjugated goat anti-human IgG or anti-human IgM. The UCAs were compared for binding to NANP18 and NPDP15 at a concentration of 22 μg ml^{-1} (Supplementary Fig. 6f).

Surface plasmon resonance (SPR) assays

Biotinylated NPDP15 and NANP18 peptides were diluted (20 nM) in HEPES buffered saline (HBS) (10 mM HEPES, pH 7.4, 150 mM NaCl, 3 mM EDTA, 0.005% surfactant Tween-20). HBS was also used as running buffer. An irrelevant biotinylated 19-mer peptide was used as a control for non-specific interactions. A NeutrAvidin-immobilized NLC ProteOn sensor chip (Biorad) was pre-conditioned with an NaCl solution (1 M) and the biotinylated peptides were injected onto the chip. The monoclonal antibodies were diluted and titrated in HBS (50-16.7-5.6-1.9-0.6 nM) and injected onto chip; one channel of the chip was injected with HBS and used as reference for the analysis. All injections were made at a flow rate of 100 μl/min. Injection time and dissociation time were 240 s and 900 s, respectively. Each binding interaction of the monoclonal antibodies with the biotinylated peptides was assessed using a ProteON XPR36 instrument (Biorad) and data were processed with ProteOn Manager Software (version 3.1.0.6). K_a, K_d and K_D were calculated by applying the Langmuir fit model.

Peptide array analysis

Peptides of 15-amino acid lengths spanning the entire PfCSP (with a shift of a single amino acid between peptides) were synthesized and coated onto a microarray chip (PEPperMAP® Linear Epitope Mapping, PEPperPRINT GmBH). The peptides were incubated with 1 μg ml^{-1} of monoclonal antibodies for 16 h at 4°C, followed by incubation with DyLight680-conjugated goat anti-human IgG to detect antibody binding.

Immunization of mice

Female BALB/c mice (6–9 weeks of age) were obtained from ENVIGO Laboratories. All procedures were performed in accordance with guidelines by the Swiss Federal Veterinary Office and after obtaining ethical approval from the Ufficio Veterinario Cantonale, Bellinzona, Switzerland (approval number: 332016). Keyhole limpet haemocyanin (KLH)-conjugated NPDP19 (Genscript) was reconstituted in water and formulated with 50% MF59 (Addavax, Invivogen) according to the manufacturer's instructions. Mice were immunized subcutaneously with 50 μg of peptide on day 0 and 10. Mice were bled on day 21. Recovered sera were used for staining of PfSPZ by flow cytometry and for binding to PfCSP and PfCSP peptides by ELISA.

Statistical analysis

The number of mutations in the heavy chains of IgG (n=19 antibodies) and IgM (n=65 antibodies) isolated from the Tanzanian volunteers were compared by a two-sided t-test. Results are shown as mean ± s.d.. In this test, n refers to the number of antibodies, $P = 0.002$, $t = 3.196$, $df = 82$. A two-tailed Spearman's correlation was performed to correlate invasion with binding affinity to PfSPZ (from n=1 representative experiment out of 2), $P =$

0.0037. In the *in vivo* test of the monoclonal antibodies, error bars show s.d. and were calculated from n = 4 or 5 mice for each antibody. A one-sided ANOVA with Kruskal-Wallis post test was used to compare the percentages of liver burden with that of control mice injected with irrelevant human IgG; for the ANOVA, $P = 0.0001$, F = 4.652, df1 = 9, df2 = 55. For the Kruskal-Wallis post test, the results for each individual antibody are presented as $*P \leq 0.05$, $**P \leq 0.01$, $****P < 0.0001$. A two-tailed Spearman's correlation was performed to correlate affinity for NPDP15, PfCSP, NANP18, 282–383 or PfSPZ with *in vivo* antibody efficacy (from n=1 representative experiment out of 2). $P = 0.0183$, 0.7435, 0.3125, 0.6944 and 0.7081, respectively. The confidence intervals were not determined by Prism as n<10 for each correlation. In all other cases, n refers to the number of independent experiments.

Data availability

Sequence data of the monoclonal antibodies isolated in this study will be deposited in GenBank (https://www.ncbi.nlm.nih.gov/genbank/). The X-ray structure factors and coordinates have been deposited in the Protein Data Bank (PDB ID 6BQB).

Supplementary Material

Refer to Web version on PubMed Central for supplementary material.

Acknowledgments

We would like to thank M. Nussenzweig (Rockefeller University) and H. Wardemann (German Cancer Research Center) for providing reagents for antibody cloning and expression. This work was supported in part by the Swiss Vaccine Research Institute, by the European Research Council (grant no. 670955 BROADimmune) and by the Fondazione Aldo e Cele Daccò. J. Tan is funded by the Wellcome Trust (grant no. 204689/Z/16/Z). B. Sack is funded by the NIH (grant no. F32 AI 114113). D. Oyen and I.A. Wilson are funded by PATH's Malaria Vaccine Initiative under a collaborative agreement with The Scripps Research Institute and by the Bill and Melinda Gates Foundation. A. Lanzavecchia and F. Sallusto are supported by the Helmut Horten Foundation. This research used resources of the Advanced Light Source, which is a DOE Office of Science User Facility under contract no. DE-AC02-05CH11231. The Tanzanian Commission on Science and Technology (COSTECH), the Ifakara Health Institute, and the Swiss Tropical Public Health Institute provided funding for the clinical trial. The functional assays were supported by the Bill and Melinda Gates foundation (Investment ID: 24922). The development, manufacturing, and quality control release and stability studies of PfSPZ Vaccine and PfSPZ Challenge were supported in part by NIAID Small Business Innovation Research grant 5R44AI055229. Sanaria supported transport of PfSPZ Vaccine and PfSPZ Challenge to the study site and syringe preparation. The authors would like to thank first and foremost the study volunteers for their participation in the study. We also thank the entire study team at the Bagamoyo branch of the Ifakara Health Institute and the manufacturing, quality control, regulatory and clinical teams at Sanaria, Inc. for their contributions to the conduct of the trial. We would like to thank Prof. Marcel Tanner (former director of the Swiss Tropical and Public Health Institute, Basel) for his vision and support of the development of the clinical trial platform enabling whole sporozoite-based malaria vaccine trials in Bagamoyo, Tanzania.

References

1. World Health Organization. World malaria report 2016. 2017.
2. Hoffman S, et al. Naturally acquired antibodies to sporozoites do not prevent malaria: vaccine development implications. Science. 1987; 237:639–642. [PubMed: 3299709]
3. Tran TM, et al. An intensive longitudinal cohort study of Malian children and adults reveals no evidence of acquired immunity to *Plasmodium falciparum* infection. Clin Infect Dis. 2013; 57:40–47. [PubMed: 23487390]
4. Casares S, Brumeanu TD, Richie TL. The RTS,S malaria vaccine. Vaccine. 2010; 28:4880–4894. [PubMed: 20553771]

5. Dups JN, Pepper M, Cockburn IA. Antibody and B cell responses to *Plasmodium* sporozoites. 2014; 5:625.
6. Ishizuka AS, et al. Protection against malaria at 1 year and immune correlates following PfSPZ vaccination. Nat Med. 2016; 22:614–623. [PubMed: 27158907]
7. Cerami C, et al. The basolateral domain of the hepatocyte plasma membrane bears receptors for the circumsporozoite protein of *Plasmodium falciparum* sporozoites. Cell. 1992; 70:1021–1033. [PubMed: 1326407]
8. Frevert U, et al. Malaria circumsporozoite protein binds to heparan sulfate proteoglycans associated with the surface membrane of hepatocytes. J Exp Med. 1993; 177:1287–1298. [PubMed: 8478608]
9. Coppi A, Pinzon-Ortiz C, Hutter C, Sinnis P. The *Plasmodium* circumsporozoite protein is proteolytically processed during cell invasion. J Exp Med. 2005; 201:27–33. [PubMed: 15630135]
10. RTSS Clinical Trials Partnership. Efficacy and safety of RTS S/AS01 malaria vaccine with or without a booster dose in infants and children in Africa: final results of a phase 3 individually randomised controlled trial. Lancet. 2015; 386:31–45. [PubMed: 25913272]
11. Coppi A, et al. Heparan sulfate proteoglycans provide a signal to *Plasmodium* sporozoites to stop migrating and productively invade host cells. Cell Host Microbe. 2007; 2:316–327. [PubMed: 18005753]
12. Coppi A, et al. The malaria circumsporozoite protein has two functional domains, each with distinct roles as sporozoites journey from mosquito to mammalian host. J Exp Med. 2011; 208:341–356. [PubMed: 21262960]
13. Olotu A, et al. Four-year efficacy of RTS,S/AS01E and its interaction with malaria exposure. N Engl J Med. 2013; 368:1111–1120. [PubMed: 23514288]
14. Olotu A, et al. Seven-year efficacy of RTS,S/AS01 malaria vaccine among young African children. N Engl J Med. 2016; 374:2519–2529. [PubMed: 27355532]
15. Nussenzweig RS, Vanderberg J, Most H, Orton C. Protective immunity produced by the injection of X-irradiated sporozoites of *Plasmodium berghei*. Nature. 1967; 216:160–162. [PubMed: 6057225]
16. Clyde DF, Most H, McCarthy VC, Vanderberg JP. Immunization of man against sporozoite-induced falciparum malaria. Am J Med Sci. 1973; 266:169–177. [PubMed: 4583408]
17. Rieckmann KH, Carson PE, Beaudoin RL, Cassells JS, Sell KW. Sporozoite induced immunity in man against an Ethiopian strain of *Plasmodium falciparum*. Trans R Soc Trop Med Hyg. 1974; 68:258–259. [PubMed: 4608063]
18. Hoffman SL, et al. Protection of humans against malaria by immunization with radiation-attenuated *Plasmodium falciparum* sporozoites. J Infect Dis. 2002; 185:1155–1164. [PubMed: 11930326]
19. Hoffman SL, et al. Development of a metabolically active, non-replicating sporozoite vaccine to prevent *Plasmodium falciparum* malaria. Hum Vaccin. 2010; 6:97–106. [PubMed: 19946222]
20. Seder RA, et al. Protection against malaria by intravenous immunization with a nonreplicating sporozoite vaccine. Science. 2013; 341:1359–1365. [PubMed: 23929949]
21. Mordmüller B, et al. Sterile protection against human malaria by chemoattenuated PfSPZ vaccine. Nature. 2017; 542:445–449. [PubMed: 28199305]
22. Sissoko M, et al. Safety and efficacy of PfSPZ Vaccine against *Plasmodium falciparum* via direct venous inoculation in healthy malaria-exposed adults in Mali: a randomised, double-blind phase 1 trial. Lancet Infect Dis. 2017; 17:498–509. [PubMed: 28216244]
23. Zavala F, et al. Rationale for development of a synthetic vaccine against *Plasmodium falciparum* malaria. Science. 1985; 228:1436–1440. [PubMed: 2409595]
24. Arun Kumar K, et al. The circumsporozoite protein is an immunodominant protective antigen in irradiated sporozoites. Nature. 2006; 444:937–940. [PubMed: 17151604]
25. Triller G, et al. Natural parasite exposure induces protective human anti-malarial antibodies. Immunity. 2017; 47:1–13. [PubMed: 28723543]
26. Dyson HJ, Satterthwait AC, Lerner RA, Wright PE. Conformational preferences of synthetic peptides derived from the immunodominant site of the circumsporozoite protein of *Plasmodium falciparum* by 1H NMR. Biochemistry. 1990; 29:7828–7837. [PubMed: 2261440]

27. Ghasparian A, Moehle K, Linden A, Robinson JA. Crystal structure of an NPNA-repeat motif from the circumsporozoite protein of the malaria parasite *Plasmodium falciparum*. Chem Commun. 2006; 365:174–176.
28. Oyen D, et al. Structural basis for antibody recognition of the NANP repeats in *Plasmodium falciparum* circumsporozoite protein. Proc Natl Acad Sci USA. 2017; 114:E10438–E10445. [PubMed: 29138320]
29. Fisher CR, et al. T-dependent B cell responses to *Plasmodium* induce antibodies that form a high-avidity multivalent complex with the circumsporozoite protein. PLoS Pathog. 2017; 13:e1006469–23. [PubMed: 28759640]
30. Hernandez EC, Suarez CF, Parra CA, Patarroyo MA, Patarroyo ME. Identification of five different IGHV gene families in owl monkeys (*Aotus nancymaae*). Tissue Antigens. 2005; 66:640–649. [PubMed: 16305680]
31. Krishnamurty AT, et al. Somatically hypermutated *Plasmodium*-specific IgM^+ memory B cells are rapid, plastic, early responders upon malaria rechallenge. Immunity. 2016; 45:402–414. [PubMed: 27473412]
32. Weill JC, Weller S, Reynaud CA. Human marginal zone B cells. Annu Rev Immunol. 2009; 27:267–285. [PubMed: 19302041]
33. Lindner SE, et al. Total and putative surface proteomics of malaria parasite salivary gland sporozoites. Mol Cell Proteomics. 2013; 12:1127–1143. [PubMed: 23325771]
34. Swearingen KE, et al. Interrogating the *Plasmodium* sporozoite surface: identification of surface-exposed proteins and demonstration of glycosylation on CSP and TRAP by mass spectrometry-based proteomics. PLoS Pathog. 2016; 12:e1005606. [PubMed: 27128092]
35. Rathore D, et al. An immunologically cryptic epitope of *Plasmodium falciparum* circumsporozoite protein facilitates liver cell recognition and induces protective antibodies that block liver cell invasion. J Biol Chem. 2005; 280:20524–20529. [PubMed: 15781464]
36. Bongfen SE, et al. The N-terminal domain of *Plasmodium falciparum* circumsporozoite protein represents a target of protective immunity. Vaccine. 2009; 27:328–335. [PubMed: 18984024]
37. Espinosa DA, et al. Proteolytic cleavage of the *Plasmodium falciparum* circumsporozoite protein is a target of protective antibodies. J Infect Dis. 2015; 212:1111–1119. [PubMed: 25762791]
38. Tissot AC, et al. Versatile virus-like particle carrier for epitope based vaccines. PLoS ONE. 2010; 5:e9809. [PubMed: 20352110]
39. Hsia Y, et al. Design of a hyperstable 60-subunit protein icosahedron. Nature. 2016; 535:136–139. [PubMed: 27309817]
40. Pappas L, et al. Rapid development of broadly influenza neutralizing antibodies through redundant mutations. Nature. 2014; 516:418–422. [PubMed: 25296253]
41. Joyce MG, et al. Vaccine-induced antibodies that neutralize group 1 and group 2 influenza A viruses. Cell. 2016; 166:609–623. [PubMed: 27453470]
42. Charoenvit Y, et al. Monoclonal, but not polyclonal, antibodies protect against *Plasmodium yoelii* sporozoites. J Immunol. 1991; 146:1020–1025. [PubMed: 1988490]
43. Charoenvit Y, et al. Inability of malaria vaccine to induce antibodies to a protective epitope within its sequence. Science. 1991; 251:668–671. [PubMed: 1704150]
44. Sack BK, et al. Humoral protection against mosquito bite-transmitted P*lasmodium falciparum* infection in humanized mice. NPJ Vaccines. 2017; 2:27. [PubMed: 29263882]
45. Roggero MA, et al. Synthesis and immunological characterization of 104-mer and 102-mer peptides corresponding to the N- and C-terminal regions of the *Plasmodium falciparum* CS protein. Mol Immunol. 1995; 32:1301–1309. [PubMed: 8643099]
46. Chen VB, et al. MolProbity: all-atom structure validation for macromolecular crystallography. Acta Crystallogr D Biol Crystallogr. 2010; 66:12–21. [PubMed: 20057044]
47. Traggiai E, et al. An efficient method to make human monoclonal antibodies from memory B cells: potent neutralization of SARS coronavirus. Nat Med. 2004; 10:871–875. [PubMed: 15247913]
48. Kaushansky A, Rezakhani N, Mann H, Kappe SHI. Development of a quantitative flow cytometry-based assay to assess infection by *Plasmodium falciparum* sporozoites. Mol Biochem Parasitol. 2012; 183:100–103. [PubMed: 22342965]

49. Tiller T, et al. Efficient generation of monoclonal antibodies from single human B cells by single cell RT-PCR and expression vector cloning. J Immunol Methods. 2008; 329:112–124. [PubMed: 17996249]
50. Lefranc MP, et al. IMGT, the international ImMunoGeneTics information system. Nucleic Acids Res. 2009; 37:D1006–12. [PubMed: 18978023]
51. Goujon M, et al. A new bioinformatics analysis tools framework at EMBL-EBI. Nucleic Acids Res. 2010; 38:W695–W699. [PubMed: 20439314]
52. Kepler TB. Reconstructing a B-cell clonal lineage. I. Statistical inference of unobserved ancestors. F1000Res. 2013; 2:103. [PubMed: 24555054]
53. Liao HX, et al. Co-evolution of a broadly neutralizing HIV-1 antibody and founder virus. Nature. 2013; 496:469–476. [PubMed: 23552890]
54. Otwinowski Z, Minor W. Processing of X-ray diffraction data collected in oscillation mode. Meth Enzymol. 1997; 276:307–326.
55. McCoy AJ, et al. Phaser crystallographic software. J Appl Crystallogr. 2007; 40:658–674. [PubMed: 19461840]
56. Biasini M, et al. SWISS-MODEL: modelling protein tertiary and quaternary structure using evolutionary information. Nucleic Acids Res. 2014; 42:W252–8. [PubMed: 24782522]
57. Bordoli L, et al. Protein structure homology modeling using SWISS-MODEL workspace. Nat Protoc. 2009; 4:1–13. [PubMed: 19131951]
58. Arnold K, Bordoli L, Kopp J, Schwede T. The SWISS-MODEL workspace: a web-based environment for protein structure homology modelling. Bioinformatics. 2006; 22:195–201. [PubMed: 16301204]
59. Lepore R, Olimpieri PP, Messih MA, Tramontano A. PIGSPro: prediction of immunoGlobulin structures v2. Nucleic Acids Res. 2017; 45:W17–W23. [PubMed: 28472367]
60. Adams PD, et al. PHENIX: a comprehensive Python-based system for macromolecular structure solution. Acta Crystallogr D Biol Crystallogr. 2010; 66:213–221. [PubMed: 20124702]
61. Emsley P, Lohkamp B, Scott WG, Cowtan K. Features and development of Coot. Acta Crystallogr D Biol Crystallogr. 2010; 66:486–501. [PubMed: 20383002]
62. Connolly ML. The molecular surface package. J Mol Graph. 1993; 11:139–141. [PubMed: 8347567]
63. Gelin BR, Karplus M. Side-chain torsional potentials: effect of dipeptide, protein, and solvent environment. Biochemistry. 1979; 18:1256–1268. [PubMed: 427111]

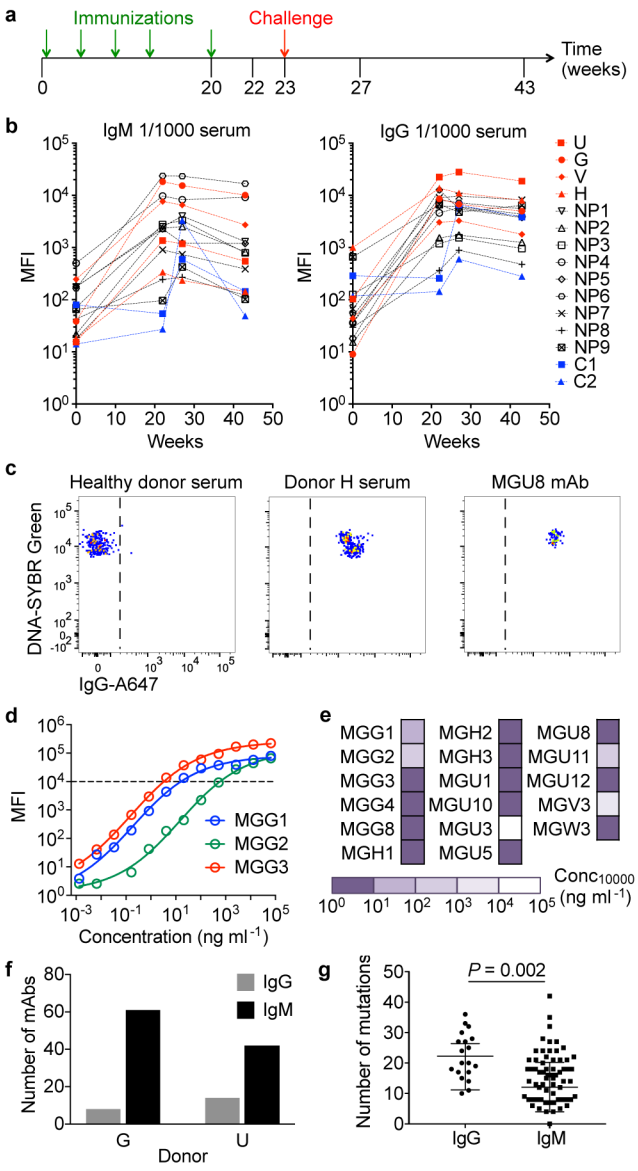

Figure 1. Immunization with PfSPZ Vaccine induces robust antibody responses in malaria-exposed individuals

a, Protocol of PfSPZ immunization of Tanzanian adults. **b,** Binding of serum IgM and IgG antibodies to PfSPZ. Median fluorescence intensity (MFI) values are for binding at a 1/1000 serum dilution (representative of n=2 independent experiments). Samples in red, black and blue are from protected (U, G, V, H), non-protected (NP) and placebo (C) volunteers, respectively. Results for donor W are not shown as this donor was immunized with a lower dose of PfSPZ. **c,** Staining of PfSPZ by serum from a European blood donor, serum from a protected individual (donor H) and a monoclonal antibody (MGU8) (representative of n=3 independent experiments). **d,** Dose-dependent binding of three representative antibodies to PfSPZ measured by flow cytometry (representative of n=2 independent experiments). **e,** Binding values of the panel of IgG monoclonal antibodies to PfSPZ (representative of n=2 independent experiments). The values indicate the concentration of antibody required to

reach a 10,000 MFI. **f,** Number of PfSPZ-binding IgG and IgM monoclonal antibodies isolated from protected donors G and U. **g,** Number of mutations in the heavy chains of IgG (n=19 antibodies) and IgM (n=65 antibodies) isolated from the Tanzanian volunteers. These values were calculated by adding the number of VH and JH mutations. Results are shown as mean ± s.d.. A two-sided t-test was used to compare the number of mutations.

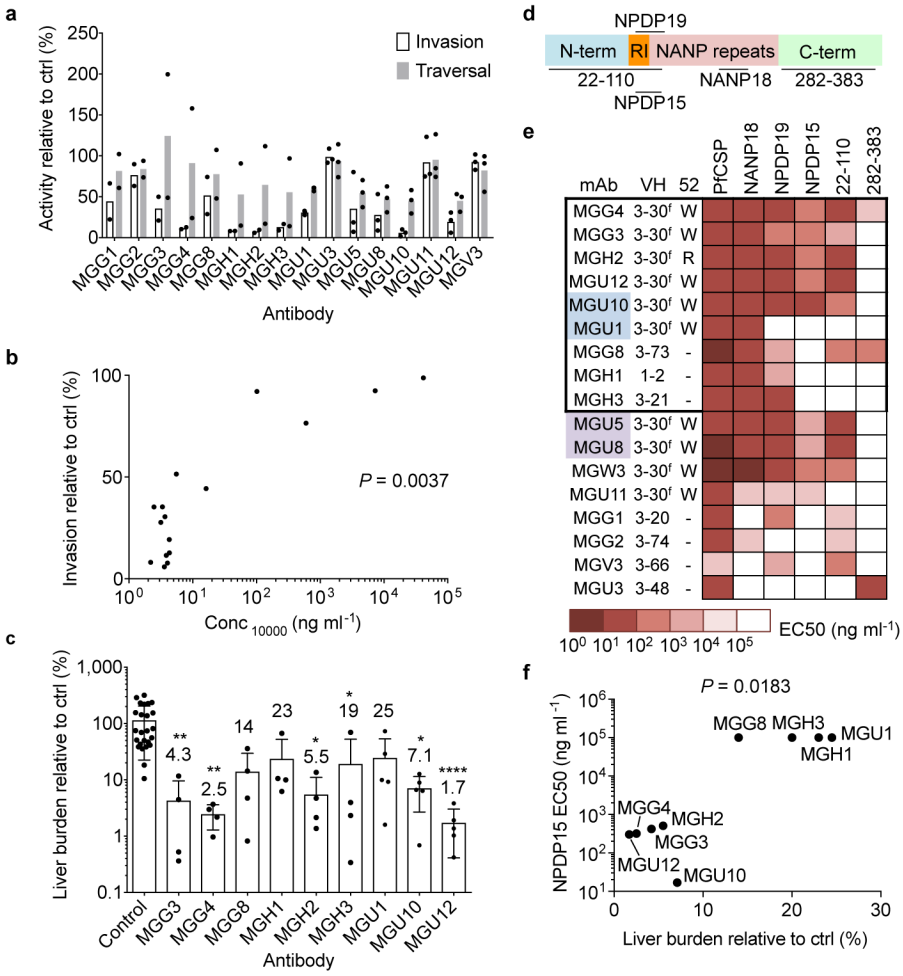

Figure 2. Highly neutralizing antibodies use VH3-30^{f} genes and exhibit dual specificity for NANP and the N-terminus junction

a, *In vitro* inhibition of PfSPZ traversal and invasion by monoclonal antibodies (n=2 or 3 independent experiments). Bars show mean percentages relative to control experiments with irrelevant human IgG. **b,** Correlation of invasion with binding affinity to PfSPZ (from n=1 representative experiment out of 2). A two-tailed Spearman's correlation was performed, 95% confidence interval 0.2878–0.8887. **c,** *In vivo* activity of monoclonal antibodies in humanized liver mice infected by *P. falciparum* via mosquito bites (n = 4 or 5 mice per antibody tested). Bars show the mean percentage of liver parasite burden relative to that of control mice injected with irrelevant human IgG. Error bars show s.d.. A one-sided ANOVA with Kruskal-Wallis test was used; *$P \leq 0.05$, **$P \leq 0.01$, ****$P < 0.0001$. **d,** Scheme of PfCSP (not to scale). **e,** Binding of monoclonal antibodies to full-length PfCSP and PfCSP peptides (representative of n=2 independent experiments). The antibodies are classified according to the VH gene used and the residue at position 52 for VH3-30^{f} antibodies. The antibodies in the box are those tested in the *in vivo* assay. Antibodies belonging to the same clone are highlighted in the same colour. NANP18, NANPNANPNANPNANPNA; NPDP15, KQPADGNPDPNANPN; NPDP19, KQPADGNPDPNANPNVDPN. 22-110 and 282-383 are long N-terminal and C-terminal peptides from Pf3D7 CSP, respectively[36,45]. **f,**

Correlation of affinity for NPDP15 with *in vivo* antibody efficacy. A two-tailed Spearman's correlation was performed (from n=1 representative experiment out of 2). Confidence interval not determined by Prism for n<10.

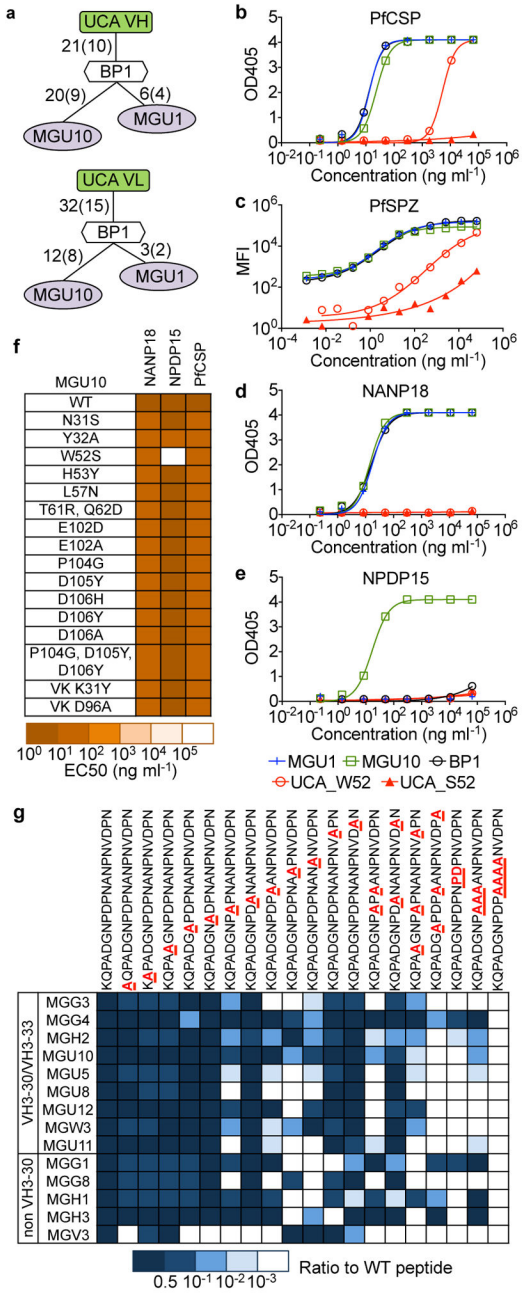

Figure 3. Somatic mutations increase affinity for PfCSP and lead to the acquisition of dual specificity

a, VH and VL genealogy trees of MGU1 and MGU10. Shown are the nucleotide and amino acid substitutions, with the latter in parentheses. UCA, unmutated common ancestor; BP, branch point. **b–e,** Binding of members of the MGU1 and MGU10 clonal family to PfCSP, PfSPZ, NANP18, and NPDP15, respectively (representative of n=2 independent experiments). **f,** Binding of MGU10 mutants to NANP18, NPDP15 and full-length PfCSP (representative of n=2 independent experiments). **g,** Binding of monoclonal antibodies to

NPDP19 peptide mutants (n=1 experiment). The letters highlighted in red show the mutated residues in the peptide.

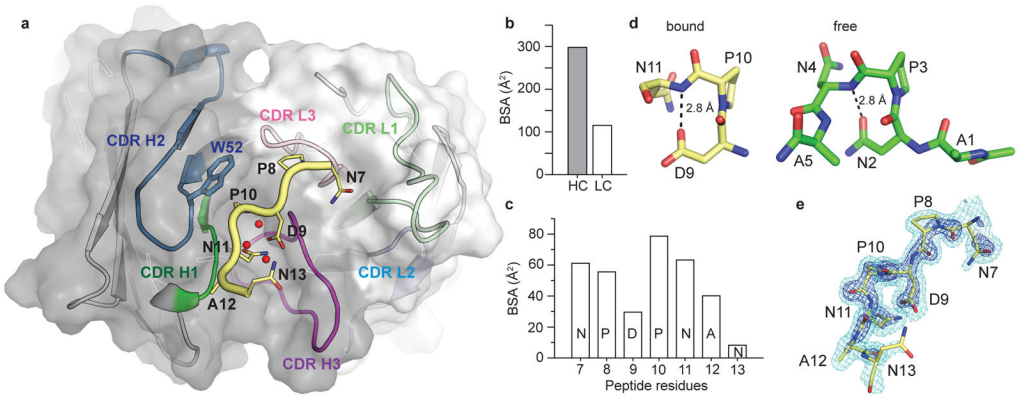

Figure 4. Structural basis for recognition of an N-terminal junctional peptide by MGG4

a, Binding interface of MGG4 in complex with the ^{1}KQPADG**NPDPNAN**P^{14} peptide; only residues 7 to 13 of the peptide have interpretable electron density (indicated in bold). The peptide is shown in the cartoon representation with sidechains as sticks, while the heavy and light chains of MGG4 are shown as dark and light grey surfaces respectively. The CDR loops are in the cartoon representation: CDRH1 (green), CDRH2 (blue), CDRH3 (magenta), CDRL1 (light green), CDRL2 (light blue) and CDRL3 (pink). The W52 sidechain is shown as blue sticks and the interfacial waters are highlighted as red spheres. **b,** Buried surface area (BSA) for the heavy chain (HC) and light chain (LC) with the peptide. **c,** BSA for individual peptide residues with the Fab. **d,** Pseudo 3_{10} turn for the DPN motif of the bound peptide (yellow carbons) and type I β-turn for the previously published crystal structure of the unbound ANPNA peptide (green carbons)[27]. Stabilizing hydrogen bonds between the sidechain of D9/N2 and the amide backbone of N11/N4 in the two structures are highlighted by the dashed line. **e,** 2Fo-Fc electron density map for the N-terminal peptide contoured at 2.0σ (dark blue) and 0.8σ (light blue).